

Article

Integrating a Top-Gas Recycling and CO₂ Electrolysis Process for H₂-Rich Gas Injection and Reduce CO₂ Emissions from an Ironmaking Blast Furnace

Yichao Hu ¹, Yinxuan Qiu ¹, Jian Chen ², Liangyuan Hao ³, Thomas Edward Rufford ¹, Victor Rudolph ¹ and Geoff Wang ^{1,*}

¹ School of Chemical Engineering, The University of Queensland, St. Lucia 4072, Australia; h.yichao@uq.edu.au (Y.H.); yinxuan.qiu@uq.edu.au (Y.Q.); t.rufford@uq.edu.au (T.E.R.); v.rudolph@uq.edu.au (V.R.)

² College of Mechanical and Electrical Engineering, Central South University, Changsha 410083, China; chenj@csu.edu.cn

³ The Strategy Research Institute, HBIS Group Co., Ltd., Shijiazhuang 050023, China; haoliangyuan@hbisco.com

* Correspondence: gxwang@uq.edu.au

Abstract: Introducing CO₂ electrochemical conversion technology to the iron-making blast furnace not only reduces CO₂ emissions, but also produces H₂ as a byproduct that can be used as an auxiliary reductant to further decrease carbon consumption and emissions. With adequate H₂ supply to the blast furnace, the injection of H₂ is limited because of the disadvantageous thermodynamic characteristics of the H₂ reduction reaction in the blast furnace. This paper presents thermodynamic analysis of H₂ behaviour at different stages with the thermal requirement consideration of an iron-making blast furnace. The effect of injecting CO₂ lean top gas and CO₂ conversion products H₂–CO gas through the raceway and/or shaft tuyeres are investigated under different operating conditions. H₂ utilisation efficiency and corresponding injection volume are studied by considering different reduction stages. The relationship between H₂ injection and coke rate is established. Injecting 7.9–10.9 m³/tHM of H₂ saved 1 kg/tHM coke rate, depending on injection position. Compared with the traditional blast furnace, injecting 80 m³/tHM of H₂ with a medium oxygen enrichment rate (9%) and integrating CO₂ capture and conversion reduces CO₂ emissions from 534 to 278 m³/tHM. However, increasing the hydrogen injection amount causes this iron-making process to consume more energy than a traditional blast furnace does.

Keywords: blast furnace; hydrogen injection; gas utilisation efficiency; energy consumption; CO₂ emission



Citation: Hu, Y.; Qiu, Y.; Chen, J.; Hao, L.; Rufford, T.E.; Rudolph, V.; Wang, G. Integrating a Top-Gas Recycling and CO₂ Electrolysis Process for H₂-Rich Gas Injection and Reduce CO₂ Emissions from an Ironmaking Blast Furnace. *Materials* **2022**, *15*, 2008. <https://doi.org/10.3390/ma15062008>

Academic Editor: Miguel Ángel Sanjuán

Received: 31 January 2022

Accepted: 6 March 2022

Published: 8 March 2022

Publisher's Note: MDPI stays neutral with regard to jurisdictional claims in published maps and institutional affiliations.



Copyright: © 2022 by the authors. Licensee MDPI, Basel, Switzerland. This article is an open access article distributed under the terms and conditions of the Creative Commons Attribution (CC BY) license (<https://creativecommons.org/licenses/by/4.0/>).

1. Introduction

Traditional blast furnace (BF) iron making relies on carbon and contributes to over 70% of CO₂ emissions in the iron and steel industry [1]. In a blast furnace, coke is converted into a high-temperature CO gas and performs an exothermic reaction with iron ores, resulting in a large amount of CO and CO₂ leaving the furnace with top gas. Typically, every tonne of hot metal (tHM) produced from a traditional BF requires about 500 kg/tHM carbon and generates around 1.2 tonnes of CO₂ emissions [2,3]. Hence, there were various attempts for a clean iron-making process to reduce CO₂ emissions [4–7]. One of the approaches is using alternative reductants produced from renewable energies to replace carbon. BF operation with hydrogen as an auxiliary reducing agent was extensively investigated because of its specific advantages over CO [8–12]. Compared to CO reduction that generates CO₂, reducing iron ores by hydrogen only forms water vapor. Kinetically, hydrogen enables a higher gas flow rate, and a faster reduction in iron ores and productivity than only CO does [13,14]. The higher thermal conductivity of hydrogen helps in heat transfer efficiency between solid and gas phases [15]. In addition, the hydrogen reduction in iron

ores suppresses the strong endothermic direct reduction in iron ores. However, hydrogen reduction is thermally more disadvantageous than CO reduction. Due to this endothermic reduction in iron ores by hydrogen, hydrogen addition changes the energy supply of the BF, and it is only useful to a certain extent [16–18].

Few previous experiments and mathematical models have investigated the maximal or optimal hydrogen injection to the BF, and results are controversial and need further investigation. A thermogravimetric experiment showed the efficiency of hydrogen on reduction rate is neglected when its content is lower than 5%, and H₂ content should be 5% to 15% at reduction temperatures between 700 and 1000 °C [13,19]. Wang et al. performed a pulverisation experiment at 900 °C with 70% N₂ and found that the reduction degree of burdens was more than 90% when H₂ content was higher than 20% [20]. On the basis of reduction experiments, Lyu et al. reported that the appropriate H₂ content lies between 5% to 10% in terms of the reduction rate, gas utilisation, and reasonable distribution of the energy in the BF in the CO and H₂ mixture [17]. Nogami et al. used a multiphase fluid dynamic model to simulate the effect of hydrogen injection with 2.5% oxygen enrichment [8]. They demonstrated that the coke rate decreases linearly, and the maximal hydrogen injection can reach 43.7%.

The application of hydrogen in large-scale BF iron-making processes is limited due to its supply in terms of cost, availability, storage, and transportation [21,22]. The traditional BF contains a low level of hydrogen content because it only generates from the blast air moisture and the volatiles of pulverised coal. One opportunity for BF hydrogen enrichment is injecting hydrogen-rich (so-called H₂-rich) gas or hydrogen-bearing materials from external sources, including natural gas, fuel oil, coke oven gas (COG), reformed gas, and waste plastics (C_nH_m) [23–26]. Previous studies adopted photocatalysis to produce CO and H₂ from CO₂. However, the productivity of photocatalysis is less than 1000 μmol CO/gCO₂ and 19 μmol H₂/gCO₂ [27,28]. It is challenging for photocatalysis to meet the large-scale CO₂ conversion requirement in the iron-making process. Electrochemical CO₂ conversion is one option that can recycle carbon into blast furnace gas (BFG) as CO [29]. The high energy demand is considered to be a major difficulty for electrochemical reduction in CO₂ [30]. However, it provides an added opportunity for a BF because hydrogen is coproduced in the electrolyser, which can be used for iron-ore reduction. In low-temperature electrolysis cells, CO₂ reduction is carried out in aqueous solutions, and different levels of current density can be used to produce hydrogen at various concentrations [31–33]. As an additional benefit, a pure oxygen stream is generated as another byproduct during electrolysis, which can be used directly for oxygen enrichment to the BF [34]. In this study, we use CO₂ capture and utilisation (CCU) technology to provide a reliable on-site H₂-rich gas for the BF iron-making process while avoiding CO₂ emissions. Renewable energy can be coupled to CO₂ electrolysis to achieve further emission reduction.

This study aims to use a modelling method to predict hydrogen involvement in the BF and determine the CO₂ emission reduction potential. An alternative method to determine the hydrogen utilisation efficiency is developed. First, thermodynamic and thermal balance models are introduced; then, hydrogen injection is quantitatively studied to determine the optimal injection position and volume by considering key BF performance indices. Lastly, the effect of hydrogen injection on coke consumption, gas utilisation efficiency, and the energy consumption of the iron-making system are investigated.

2. Materials and Methods

Here, we studied the effect of H₂-rich gas injection through BF tuyeres at the raceway position and/or shaft tuyeres, as shown in Figure 1. The BF is studied as the main subsystem when changing the hydrogen injection condition. The CCU and gas heating subsystem is used as a black box to provide necessary input information to BF. The BFG composition and flow rate from BF are the input for the CCU unit, and the CCU unit provides H₂-rich reducing gas as the input to the BF. The operating conditions for this BF to produce 1 tonne hot metal (1 tHM) are listed in Table 1 and were kept constant throughout simulations. The

overall CO content in the gas injectant was maintained at 200 m³/tHM. The productivity of this BF is 238 tHM per hour.

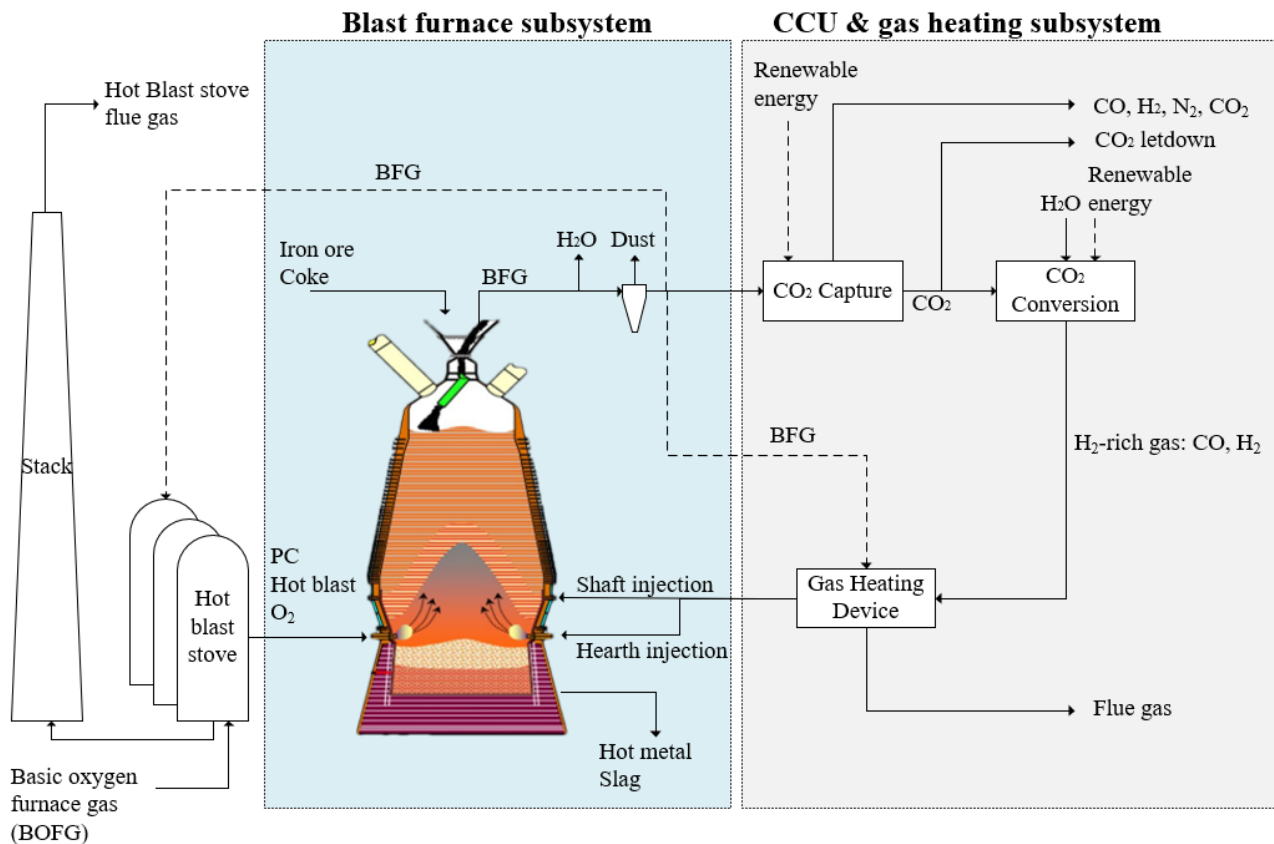


Figure 1. Blast furnace process with CO₂ capture, conversion, and H₂-rich gas injection.

Table 1. Operating conditions of the simulation.

Operating Parameters	
PCI rate (kg/tHM)	137
Blast temperature, °C	1052
Humidity of hot blast, g/m ³	12.93
Top gas temperature, °C	161
Hearth injection temperature, °C	1250
Shaft injection temperature, °C	900

As shown in Figure 1, hot oxygen-enriched blast and pulverised coal is injected through the tuyeres. The upper limit of oxygen enrichment rate for the blast was set at 14% to maintain the stable operation of the large-scale BFs. After drying and dust removal, some BFG is combusted in the hot blast stoves to heat cold blast, and in the gas heating device to provide high-temperature gas injectants. The rest of BFG enters the amine absorption CO₂ capture unit to provide a CO₂-rich stream that is processed in an electrochemical CO₂ conversion unit to produce a CO and H₂ stream containing, for example, 30% vol. H₂ and 70% vol. CO. The CO₂-lean stream from the top of the CO₂ capture unit contained a mix of CO, H₂, and N₂ that is exported to other processes in the integrated steel mill. We did not in this study consider additional separation of CO and H₂ from the N₂ in this stream for recycling back to the BF. Oxygen enrichment is required with H₂-rich gas injection to provide heat to the BF and enrich BFG for CO₂ capture [35]. The BF can take another advantage from the CCU unit, as the electrolyser produces pure oxygen in another effluent stream. Besides BFG, a small amount of the basic oxygen furnace gas (i.e., BOFG) from

steel making is usually combusted as fuel to a hot blast stove. Following assumptions of the BF, CCU unit, gas heating device and hot stove are made in this study:

- Degree of indirect reduction R_i depends on the reducing gas concentration of BF bosh gas, which is estimated by an empirical equation, as shown in Equation (1) [36]:

$$R_i = 0.2777 + 0.0051 \times \%(\text{Reducing gas}) \quad (1)$$

where $\%(\text{Reducing gas})$ is the proportion of H_2 and CO in the total amount of gas entering the bosh and shaft.

- For the amine absorption CO_2 capture unit: 30% monoethanolamine (MEA) concentration was used for CO_2 capture in this study. The capture unit recovered 90% CO_2 in BFG, and the CO_2 purity was >99%; the general thermal energy requirement for capture was assumed to be around 1000 kWh/t CO_2 (3.6 GJ/ t CO_2) [37–39]. Any additional CO_2 captured and not converted was assumed to be released as per current operation or could be sent to CO_2 storage routes, shown as CO_2 letdown in Figure 1.
- The electrochemical CO_2 conversion unit was treated in the model as a simplified input–output model. Assumptions for the material and energy balance in the CO_2 conversion unit were based on laboratory demonstration data with additional inputs from literature sources. Briefly, the model was based on multiple two-cell vapour fed electrolyser stacks with the capacity to treat 50 t CO_2 per day; further details can be found in our other report [33]. The current density of the electrolyser was altered from 2.68 V at 0 A/m² to 3.59 V at 1862 A/m² to produce the H_2 -rich gas with different H_2/CO compositions.
- The electricity consumption for CO_2 conversion is proportional to the H_2 generation, which can be estimated as in Equation (2) [33]:

$$E_{\text{conv}} = 10.75V_{H_2\text{gen}} + 1282 \quad (2)$$

where E_{conv} is the power required for the CO_2 conversion unit, kWh/tHM; $V_{H_2\text{gen}}$ is the amount of H_2 generated by the conversion unit, m³/tHM;

- efficiency of the gas heating device was 85%;
- The hot blast stove system uses two stoves on-gas and one stove on-blast, and the efficiency of the hot blast stoves was 75%.

As indicated in Figure 1, CO_2 capture and conversion units use renewable energy to avoid their own CO_2 emissions. The type of renewable power used by the industry depends on availability and cost, such as solar power [40,41]. Besides solar power, industries can use thermal–electrical materials to recover a large amount of waste heat in an integrated steel mill to provide electricity for CCU units [42]. In addition, using the lower heating value energy to generate electricity in the steel mill and the on-site power plant can help to minimise the renewable power periodic availability problem.

To achieve the objectives of this study, two mathematical models were developed. As a reducing agent, H_2 -rich gas needs to fulfil the thermodynamic requirement of the reduction reaction to capture oxygen in iron ores. H_2 -rich gas also needs to provide enough heat in the shaft for keeping an effective reduction process. First, hydrogen behaviour in different parts of the BF was analysed. A thermodynamic model for hydrogen reduction was built to determine hydrogen utilisation efficiency. This model provides a guideline of the proper hydrogen injection concentration. Then, a thermal balance model was used to limit the hydrogen injection temperature and volume.

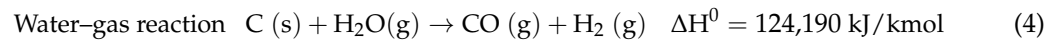
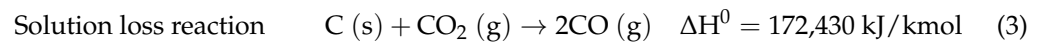
The optimal hydrogen injection amount and position were determined by increasing the reduction potential in the coke consumption and CO_2 emissions, increasing gas utilisation efficiency and lowering the energy consumption. A static mass balance model of the BF was used to calculate the above parameters.

2.1. Thermodynamic Calculations of H₂-Rich Gas Injection BF

The reduction behaviours of injected gas are discussed in different parts of the BF to determine the reducing gas utilisation.

2.1.1. Raceway

In the BF raceway, the main reactions considered in this study were carbon combustion, coke solution loss reaction between coke and CO₂, water–gas reaction between coke and moisture in the hot blast, which can be described as shown in Equations (3)–(5):



$$\Delta G^0 = 134,542 - 142.28T \quad (5)$$

With excess coke existing in the BF bottom, it could be assumed that CO and H₂ combustion was negligible. This could be justified by the assumption that, if a small amount of H₂ reacts with O₂ to form water in the raceway, the generated water vapour reacts with coke and turn back to H₂. Therefore, this process can be simplified as heating the hearth gas injectant, as shown in Equation (6):

$$\Delta Q_{\text{hearth}} = \int_{25}^{T_{\text{hearth}}} V_{\text{hearth}} \cdot C_{p_hearth} dt \quad (6)$$

where T_{hearth} is hearth gas injection temperature, °C; C_{p_hearth} denotes specific heat capacity of the gas injected to BF, kJ/m³·°C; V_{hearth} is hearth injection volume, m³/tHM; and ΔQ_{hearth} is the sensible heat carried by the gas injected to BF, kJ/tHM.

2.1.2. Dripping, Cohesive, and High-Temperature Zones over 1000 °C

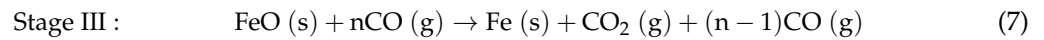
The primary reaction in the dripping zone is a direct reaction between coke and FeO. Hot gas containing H₂ and CO that passes through the cohesive zone reacts with molten FeO or semi-molten FeO to form H₂O and CO₂. As the temperature was over 1350 °C in the dripping zone, the amount of CO₂ was negligible due to the solution loss reaction. At the high-temperature zone over 1000 °C, some reduced FeO and Fe₃O₄ were still in the solid state, and H₂ could pass through their surface. Almost all the H₂O produced by H₂ reduction rapidly participates in water–gas reaction at the presence of coke to form CO and H₂ over 1273 K (1000 °C). Therefore, the reduction reaction in this section was essentially the direct reduction in iron by coke. H₂ injected through the tuyeres at the raceway mainly catalyses direct reduction and heats the molten or semi-molten burden.

2.1.3. Shaft Zone Temperature between 800 and 1000 °C

According to the thermodynamics of iron oxide reduction and dynamics studies, H₂ has better reducing capability than that of CO above 800 °C [43,44]. At the same time, the extent of coke solution loss reaction and the water–gas reaction was less than that in the higher temperature zone. In this temperature zone, H₂ reacts with various iron oxides to generate H₂O, and the formed H₂O is not gasified into H₂ by carbon completely. Therefore, it is the primary zone to improve H₂ utilisation efficiency.

The H₂-rich reducing gas utilisation rate and volume requirement vary in different ferric oxides reduction stages. The iron oxides reduction reactions are at a nonequilibrium state in the BF. When the temperature is above 570 °C, the reduction in ferric oxides by CO and H₂ in the BF occurs in the following sequences: 1/2 Fe₂O₃ → 1/3 Fe₃O₄ (Stage I) → FeO (Stage II) → Fe (Stage III) [45]. The gas produced by the reduction in the latter stage is the reducing gas for the previous stage. Heat is gradually transferred to solid materials during the gas ascending. At the same time, part of reducing gas reacts with iron oxides and converts into CO₂ and H₂O, and finally forms top gas at around 150 to 250 °C when leaving the BF. There are 25% of the total oxygen elements removed during the reduction of Fe₃O₄

into FeO, and the remaining 75% of oxygen elements were removed in reducing FeO to Fe. Therefore, the reduction process from FeO to Fe is the key step. The required reducing gas amount is n kmol for CO, and m kmol for H₂ to produce 1 kmol iron. The value of n and m is the excess coefficient. The reduction reactions and thermodynamic parameters in Stage III for CO and H₂ are expressed as in Equations (7)–(12), and Equations (13)–(17), respectively [46]:



$$\Delta H_{3\text{CO}}^0 = -13,190 \text{ kJ/kmol}$$

$$\Delta G_{3\text{CO}}^0 = -22,800 - 24.26T, \text{ kJ/kmol} \quad (8)$$

$$\ln K_{\text{III CO}} = -\frac{\Delta G_{3\text{CO}}^0}{RT} = -\frac{-22,800 - 24.26T}{RT} \quad (9)$$

$$K_{\text{III CO}} = \frac{P_{\text{CO}_2}}{P_{\text{CO}}} = \frac{\varphi_{\text{CO}_2} \times P^0}{\varphi_{\text{CO}} \times P^0} = \frac{1}{n - 1} \quad (10)$$

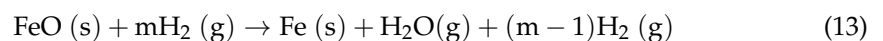
where K is the reaction equilibrium constant; φ denotes the fraction of gas component.

The minimal CO required for Stage III is described in Equation (11):

$$n = 1 + \frac{1}{K_{\text{III CO}}} \quad (11)$$

The utilisation efficiency of CO in Stage III, $\eta_{3\text{CO}}$, is described in Equation (12):

$$\eta_{3\text{CO}} = \frac{\varphi_{3\text{CO}_2}}{\varphi_{3\text{CO}} + \varphi_{3\text{CO}_2}} = \frac{1}{\frac{\varphi_{3\text{CO}}}{\varphi_{3\text{CO}_2}} + 1} = \frac{1}{\frac{1}{K_{3\text{CO}}} + 1} = \frac{K_{\text{III CO}}}{1 + K_{\text{III CO}}} = \frac{1}{n} \quad (12)$$



$$\Delta H_{3\text{H}_2}^0 = 28,010 \text{ kJ/kmol}$$

$$\Delta G_{3\text{H}_2}^0 = 23,430 - 16.16T, \text{ kJ/kmol} \quad (14)$$

$$\ln K_{\text{III H}_2} = -\frac{\Delta G_{3\text{H}_2}^0}{RT} = -\frac{23,430 - 16.16T}{RT} \quad (15)$$

The minimal H₂ required for Stage III is calculated as in Equation (16):

$$m = 1 + \frac{1}{K_{\text{III H}_2}} \quad (16)$$

The utilisation efficiency of H₂ in Stage III, $\eta_{3\text{H}_2}$ is described in Equation (17):

$$\eta_{3\text{H}_2} = \frac{\varphi_{3\text{H}_2\text{O}}}{\varphi_{3\text{H}_2} + \varphi_{3\text{H}_2\text{O}}} = \frac{K_{\text{III H}_2}}{1 + K_{\text{III H}_2}} = \frac{1}{m} \quad (17)$$

According to the theoretical thermochemical calculations, 50% of H₂ and CO participates in the water–gas shift reaction Equation (18) between 600 and 1400 °C [47]. Therefore, the heat consumed by the water–gas shift reaction at temperatures above 820 °C is balanced by the heat generated at the temperature below 820 °C, as calculated by Equation (19). However, H₂ promotes iron ore reduction by CO via the water gas shift reaction when the temperature is over 820 °C [48]. The CO₂ generated reacts with H₂ to reform CO, which participates in FeO reduction reaction again and improve the utilisation efficiency of CO.



$$\Delta H^0 = -41,325 \text{ kJ/kmol}$$

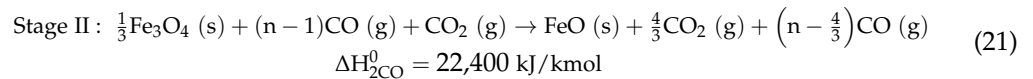
$$\Delta G^0 = -33,447 + 30.56T, \text{ kJ/kmol} \quad (19)$$

The heat effect of FeO reduction by H₂ and CO gas is calculated by Equation (20):

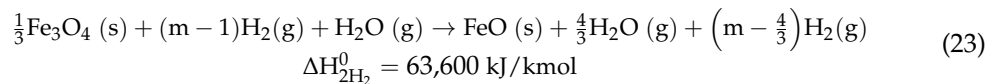
$$\Delta H = \frac{X_{\text{CO}}\eta_{3\text{CO}}\Delta H_{3\text{CO}}^0 + X_{\text{H}_2}\eta_{3\text{H}_2}\Delta H_{3\text{H}_2}^0}{X_{\text{CO}}\eta_{3\text{CO}} + X_{\text{H}_2}\eta_{3\text{H}_2}} \quad (20)$$

where X_i is the proportion of CO or H₂ in the reducing gas entering the BF shaft.

The gas produced by the reduction in Stage III is the reducing gas for Stage II. The reduction reactions and thermodynamic parameters in Stage II for CO and H₂ are expressed in Equations (21)–(28):



$$\Delta G_{2\text{CO}}^0 = 35,380 - 40.16T, \text{ kJ/kmol} \quad (22)$$



$$\Delta G_{2\text{H}_2}^0 = 71,940 - 73.62T, \text{ kJ/kmol} \quad (24)$$

$$\ln K_{\text{II CO}} = -\frac{\Delta G_{2\text{CO}}^0}{RT} = -\frac{35,380 - 40.16T}{RT} \quad (25)$$

$$\ln K_{\text{III H}_2} = -\frac{\Delta G_{2\text{H}_2}^0}{RT} = -\frac{71,940 - 73.62T}{RT} \quad (26)$$

$$K_{\text{II CO}} = \frac{\varphi_{\text{CO}_2} \times P^0}{\varphi_{\text{CO}} \times P^0} = \frac{\frac{4}{3}}{n - \frac{4}{3}} \quad (27)$$

$$K_{\text{III H}_2} = \frac{\frac{4}{3}}{m - \frac{4}{3}} \quad (28)$$

The minimal CO and H₂ volume required for Stage II is calculated as shown in Equations (29) and (30), respectively:

$$n = \frac{4}{3} \left(1 + \frac{1}{K_{\text{II CO}}} \right) \quad (29)$$

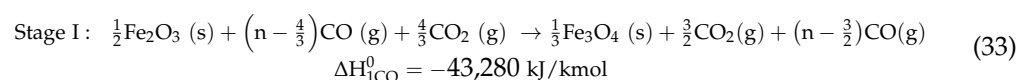
$$m = \frac{4}{3} \left(1 + \frac{1}{K_{\text{III H}_2}} \right) \quad (30)$$

The utilisation efficiency of CO and H₂ in Stage II is calculated as shown in Equations (31) and (32), respectively:

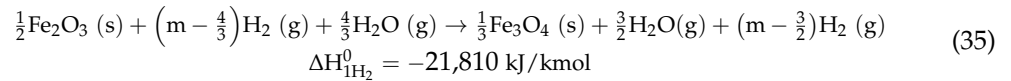
$$\eta_{2\text{CO}} = \frac{\varphi_{2\text{CO}_2}}{\varphi_{2\text{CO}} + \varphi_{2\text{CO}_2}} = \frac{K_{\text{II CO}}}{1 + K_{2\text{CO}}} = \frac{4}{3n} \quad (31)$$

$$\eta_{2\text{H}_2} = \frac{\varphi_{2\text{H}_2\text{O}}}{\varphi_{2\text{H}_2} + \varphi_{2\text{H}_2\text{O}}} = \frac{K_{\text{III H}_2}}{1 + K_{2\text{H}_2}} = \frac{4}{3m} \quad (32)$$

In the first stage of iron ores reduction, the transformation of Fe₂O₃ to Fe₃O₄ is very rapid due to the very high equilibrium constant of Fe₂O₃ reduction above 600 K, as shown in Equations (33) and (35):



$$\Delta G_{1\text{CO}}^0 = -52,131 - 41.0T, \text{ kJ/kmol} \quad (34)$$



$$\Delta G_{1\text{H}_2}^0 = -15,547 - 74.4T, \text{ kJ/kmol} \quad (36)$$

The gas produced by the reduction in Stage II provides the reducing gas for Stage I. These reactions only require a low concentration of reducing gas to proceed. The minimal CO and H₂ volume required for Stage I is shown in Equations (37) and (38), respectively. With utilisation efficiency close to 100%, Fe₂O₃ reduction is an irreversible reaction.

$$n = \frac{3}{2} \left(1 + \frac{1}{K_{\text{ICO}}}\right) \quad (37)$$

$$m = \frac{3}{2} \left(1 + \frac{1}{K_{\text{IH}_2}}\right) \quad (38)$$

The utilisation efficiency of CO and H₂ in Stage I is described by Equations (39) and (40), respectively:

$$\eta_{1\text{CO}} = \frac{\varphi_{2\text{CO}_2}}{\varphi_{2\text{CO}} + \varphi_{2\text{CO}_2}} = \frac{3}{2n} \quad (39)$$

$$\eta_{1\text{H}_2} = \frac{\varphi_{2\text{H}_2\text{O}}}{\varphi_{2\text{H}_2} + \varphi_{2\text{H}_2\text{O}}} = \frac{3}{2m} \quad (40)$$

The overall gas utilisation efficiency for H₂-rich reducing gas in the BF is calculated as in Equation (41) below:

$$\eta = \frac{\varphi_{\text{CO}_2} + \varphi_{\text{H}_2\text{O}}}{\varphi_{\text{CO}} + \varphi_{\text{CO}_2} + \varphi_{\text{H}_2} + \varphi_{\text{H}_2\text{O}}} = X_{\text{CO}}\eta_{\text{CO}} + X_{\text{H}_2}\eta_{\text{H}_2} \quad (41)$$

Assuming the water generated in the Fe₂O₃ reduction is reacted with CO, in which H₂ performs only as a catalyst of CO reduction of Fe₂O₃. The water in top gas is determined by H₂ utilisation efficiency in FeO and Fe₃O₄, which was calculated as in Equation (42):

$$V_{\text{H}_2\text{O}} = \sum V_{\text{H}_2}\eta_{3\text{H}_2} + \sum V_{\text{H}_2}(1 - \eta_{3\text{H}_2})\eta_{2\text{H}_2} + \sum V_{\text{H}_2}(1 - \eta_{3\text{H}_2})(1 - \eta_{2\text{H}_2})\eta_{1\text{H}_2} \quad (42)$$

Since FeO reduction is the key step, the theoretical overall H₂ utilisation efficiency was calculated as shown in Equation (43). The highest theoretical H₂ utilisation efficiency can be obtained with the minimal H₂ requirement value on the basis of the thermodynamic requirement in Stage III, and this highest value is determined by temperature. Due to thermal restrictions and excess H₂ injected, the actual gas utilisation efficiency can only approach this theoretical value. The actual thermodynamic utilisation efficiency of H₂ is a function of the amount of H₂ introduced to the BF, as shown in Equation (43):

$$\begin{aligned} \eta_{\text{H}_2} &= \eta_{3\text{H}_2} + (1 - \eta_{3\text{H}_2})\eta_{2\text{H}_2} + (1 - \eta_{3\text{H}_2})(1 - \eta_{2\text{H}_2})\eta_{1\text{H}_2} \\ &= \frac{1}{m} + \left(1 - \frac{1}{m}\right)\frac{4}{3m} + \left(1 - \frac{1}{m}\right)\left(1 - \frac{4}{3m}\right)\frac{3}{2m} \end{aligned} \quad (43)$$

As the FeO reduction is the key step in the indirect reduction process, the thermodynamic requirement of gas entering the BF shaft to produce 1 tHM is calculated as in Equations (44) and (45):

$$V_{\text{bosh_shaft}} = \frac{1000(\text{Fe})_{\text{HM}}(1 - R_d)}{\eta_3 \times \%(\text{Reducing gas})} \times \frac{22.4}{56} \quad (44)$$

$$R_d = 1 - R_i \quad (45)$$

where $V_{\text{bosh_shaft}}$ is the amount of gas raised from BF bosh after direct reduction and the gas injected through the shaft tuyeres, m^3/tHM ; $[\text{Fe}]_{\text{HM}}$ is the proportion of iron content in hot metal; R_d is the degree of direct reduction.

2.2. Thermal Calculations of H_2 -Rich Gas Injection BF

As the heat carrier, the H_2 -rich gas injected through raceway tuyeres needs to compensate for the required energy in the lower furnace and maintain the theoretical combustion temperature at a reasonable range. The gas injected through the shaft also needs to satisfy the heat requirement in the upper furnace. The energy of H_2 -rich gas includes the oxidation heat release from the iron ore reduction and sensible heat. The oxidation heat release depends on gas utilisation efficiency and gas composition. The injection temperature determines the sensible heat. Thermal calculations for determining the amount of H_2 -rich gas were developed by a static mass and energy model of the iron-making process.

The thermal balance for this iron-making process is developed in the lower and upper furnaces, divided by the shaft gas injection position. In this work, the lower furnace included BF raceway, dripping zone, and cohesive zone. The thermal balance of the lower furnace is shown in Equation (46) below:

$$Q_{\text{cc}} + Q_{\text{blast}} + Q_{\text{hearth}} + Q_{\text{coke}} + Q_{\text{ore}} = H_{\text{CO}_2} + H_{\text{H}_2\text{Ode}} + H_{\text{PCde}} + Q_{\text{bosh}} + H_{\text{dA}} + H_{\text{dFe}} + H_{\text{S}} + Q_{\text{HM}} + Q_{\text{slag}} + Q_{\text{loss}_1} \quad (46)$$

where the heat income in the lower furnace includes: Q_{cc} = combustion heat of coke and pulverised coal in front of tuyeres, kJ/tHM ; Q_{blast} = sensible heat of the hot blast, kJ/tHM ; Q_{hearth} = sensible heat of H_2 -rich gas injection to the hearth, kJ/tHM ; Q_{coke} = heat of the coke brings to the lower part of BF, kJ/tHM ; Q_{ore} = sensible heat of the iron ores into the lower part of the BF, kJ/tHM ; and the heat expenditure includes: H_{CO_2} = heat consumption of solution loss reaction due to the possible CO_2 in the hearth injection gas, kJ/tHM ; $H_{\text{H}_2\text{Ode}}$ = heat consumption of water decomposition in front of tuyeres, kJ/tHM ; H_{PCde} = heat consumption of pulverised coal decomposition in front of tuyeres, kJ/tHM ; Q_{bosh} = heat brought to the shaft by bosh gas, kJ/tHM ; H_{dA} = heat consumption by direct reduction of alloy element, kJ/tHM ; H_{dFe} = heat consumption by direct reduction of FeO , kJ/tHM ; H_{S} = heat consumption by desulphurisation, kJ/tHM ; Q_{HM} = sensible heat of hot metal, kJ/tHM ; Q_{slag} = sensible heat of slag, kJ/tHM ; and Q_{loss_1} = heat loss in the lower furnace, kJ/tHM .

With H_2 -rich gas injection to BF hearth, the raceway adiabatic flame temperature (RAFT) is calculated as in Equation (47):

$$\text{RAFT} = \frac{Q_{\text{coke}} + Q_{\text{blast}} + Q_{\text{hearth}} + Q_{\text{cc}} - Q_{\text{H}_2\text{Ode}} - Q_{\text{PCde}} - H_{\text{CO}_2}}{V_{\text{H}_2}^{\text{raceway}} \times C_{\text{H}_2} + V_{\text{CO}}^{\text{raceway}} \times C_{\text{CO}} + V_{\text{N}_2}^{\text{raceway}} \times C_{\text{N}_2}} \quad (47)$$

where Q_{coke} is the heat brought to the raceway by coke, kJ/tHM ; V_i^{raceway} is the gas volumes of H_2 , CO and N_2 in the raceway, m^3/tHM , respectively.

The energy input and output of the BF shaft can be expressed as in Equations (48) and (49), respectively:

$$Q_{\text{shaft}} + Q_{\text{bosh}} + Q_{\text{ind}} + Q_{\text{ore_shaft}} = Q_{\text{top}} + Q_{\text{coke}} + Q_{\text{ore}} + Q_{\text{loss}_s} \quad (48)$$

$$Q_{\text{ind}} = Q_{\text{Fe}_2\text{O}_3} + Q_{\text{Fe}_3\text{O}_4} + Q_{\text{FeO}} \quad (49)$$

where Q_{shaft} is the heat carried by H_2 -rich gas injected into the shaft, kJ/tHM ; Q_{ind} is the heat generation by iron oxides reduction by H_2 and CO , kJ/tHM ; $Q_{\text{ore_shaft}}$ is the sensible heat carried by iron ores entering the BF top, kJ/tHM ; Q_{top} , kJ/tHM is heat loss in the shaft, kJ/tHM .

The heats provided by the reduction reactions from Fe_2O_3 to Fe_3O_4 , Fe_3O_4 to FeO , and FeO to Fe by CO and H_2 are calculated as from Equations (50)–(52), respectively:

$$Q_{\text{Fe}_2\text{O}_3} = 56 \times \frac{m_{\text{ore}} \times \frac{w(\text{Fe}_2\text{O}_3)_{\text{ore}}}{160}}{3} \left(r_{\text{ico}} \times \Delta H_{1\text{CO}}^0 + r_{\text{iH}_2} \times \Delta H_{1\text{H}_2}^0 \right) \quad (50)$$

$$Q_{\text{Fe}_3\text{O}_4} = 56 \times \frac{2 \times m_{\text{ore}} \times \frac{w(\text{Fe}_2\text{O}_3)_{\text{ore}}}{160}}{3} \left(r_{\text{ico}} \times \Delta H_{2\text{CO}}^0 + r_{\text{iH}_2} \times \Delta H_{2\text{H}_2}^0 \right) \quad (51)$$

$$Q_{\text{FeO}} = 56 \times (1 - R_d) \left(\frac{2 \times m_{\text{ore}} \times w(\text{Fe}_2\text{O}_3)_{\text{ore}}}{160} + \frac{m_{\text{ore}} \times w(\text{FeO})_{\text{ore}}}{72} \right) \left(r_{\text{ico}} \times \Delta H_{3\text{CO}}^0 + r_{\text{iH}_2} \times \Delta H_{3\text{H}_2}^0 \right) \quad (52)$$

where r_{ico} and r_{iH_2} are the degree of indirect reduction by CO and H_2 , as shown in Equations (53) and (54), respectively:

$$r_{\text{iH}_2} = \frac{V_{\text{H}_2\text{O}}}{22.4 \times 1000(\text{Fe})_{\text{HM}}} \times 56 \quad (53)$$

$$r_{\text{ico}} = R_i - r_{\text{iH}_2} \quad (54)$$

3. Results and Discussion

3.1. Results of the Thermodynamic Model

At a medium oxygen enrichment rate (9%), the nitrogen content in the BF shaft is calculated at around 35%. Figure 2a shows the heat effect results based on Equation (20). The FeO reduction reaction transforms from an exothermic into an endothermic process when H_2 content increases to 25% around 900 °C. A similar phenomenon shows up when the H_2 reaches 20% around 1000 °C. With more H_2 participating in the reduction at high temperatures, it causes a severe negative effect on the thermal energy supply to the BF. Therefore, the shaft gas injection temperature should not be too high to reduce its endothermic heat effect and require less preheating in the gas preheating device. The higher oxygen enrichment (less N_2 content) enables higher H_2 content in the BF, as shown in Figure 2b. It is suggested that with 20% N_2 entering the BF shaft, the H_2 content should be lower than 25% to avoid too much heat consumption by its reduction reaction.

According to Equations (11), (16), (29) and (30), the theoretical minimal H_2 and CO requirement with temperature are shown in Figure 3. From this figure, Stage III for iron ores reduction requires more H_2 when the temperature is over 625 °C. Stage III requires more CO over 650 °C. In this study, since the gas injection temperature is kept above 820 °C to ensure the high reducing capability of H_2 , the thermodynamic key step for iron ores reduction is Stage III, and the other stages are proceeded with excess reducing gas. Compared with Fe_3O_4 , FeO reduction requires more reducing gas to proceed, which determines the minimal amount of gaseous mixture. Fe_3O_4 and Fe_2O_3 reductions are carried out with excess reducing gas. In addition, the amount of H_2 required for FeO reduction at high temperatures is less than the amount of CO required in the reaction. Thermodynamically, injecting H_2 content to replace some amount of CO would reduce the total amount of gas mixture and reduce the fuel requirement for the gas preheating. However, CO content in the BF should be enough to meet its thermal condition.

According to Figure 4, gas utilisation efficiency for H_2 and CO was similar in Stage II when the temperature was above 820 °C, but H_2 utilisation efficiency was much higher than that for CO in Stage III. Although the utilisation efficiency of CO decreases as temperature increases, the FeO reduction reaction would still be promoted with increasing H_2 content due to the effect of the water–gas shift reaction.

On the basis of the calculation from Equation (41), gas utilisation efficiency at different H_2 contents in the reducing gas for FeO and Fe_3O_4 reduction is shown in Figure 5.

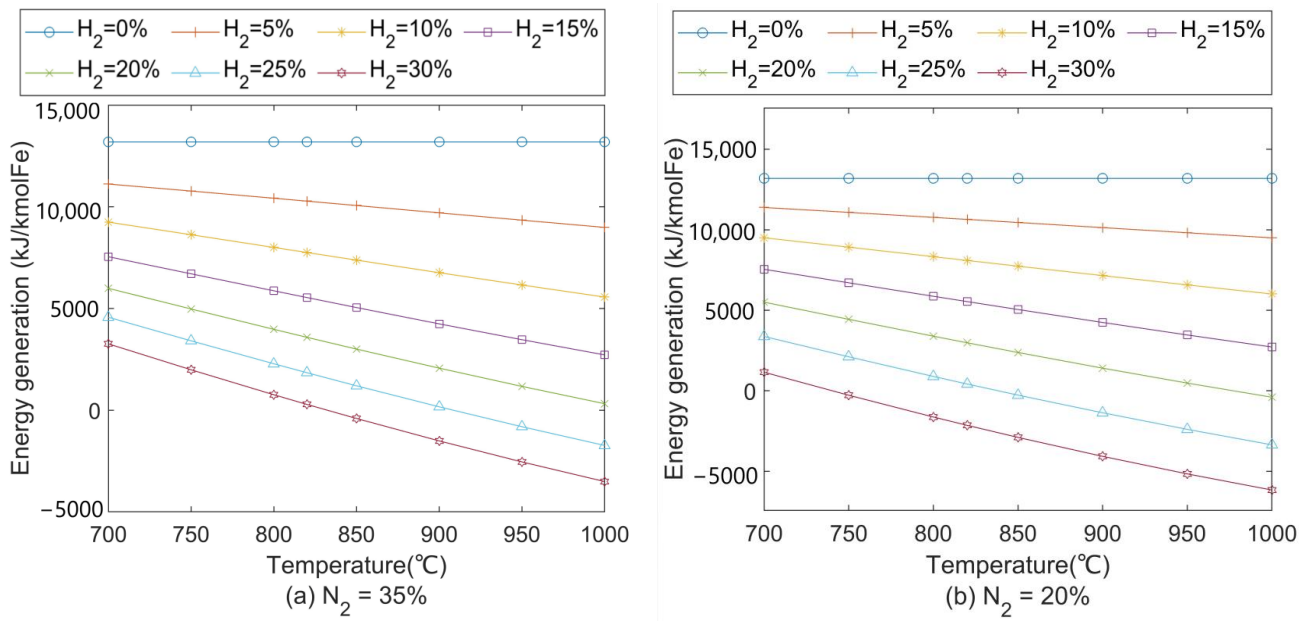


Figure 2. Heat effect of FeO reduction in H₂-CO-N₂ gas mixture at (a) 35% N₂ and (b) 20% N₂. H₂ content entering blast furnace shaft is indicated by different colours.

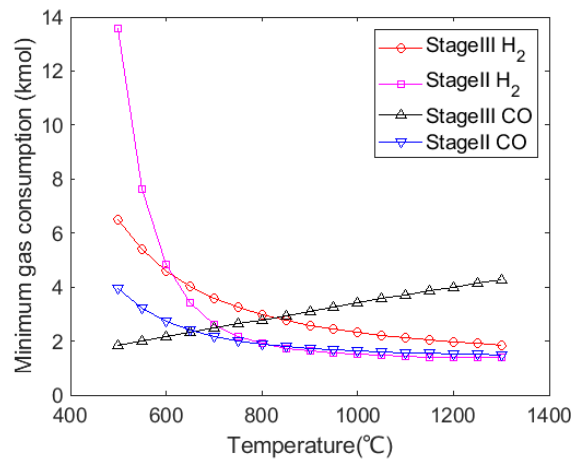


Figure 3. Variation in minimal gas consumption for iron ores reduction in pure H₂ or CO with temperature.

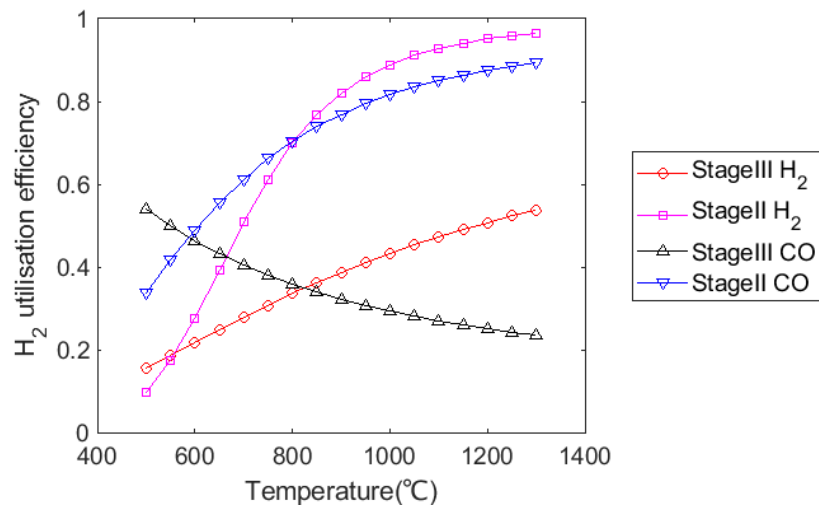


Figure 4. Variation in gas utilisation efficiency for iron ores reduction in pure H₂ or CO with temperature.

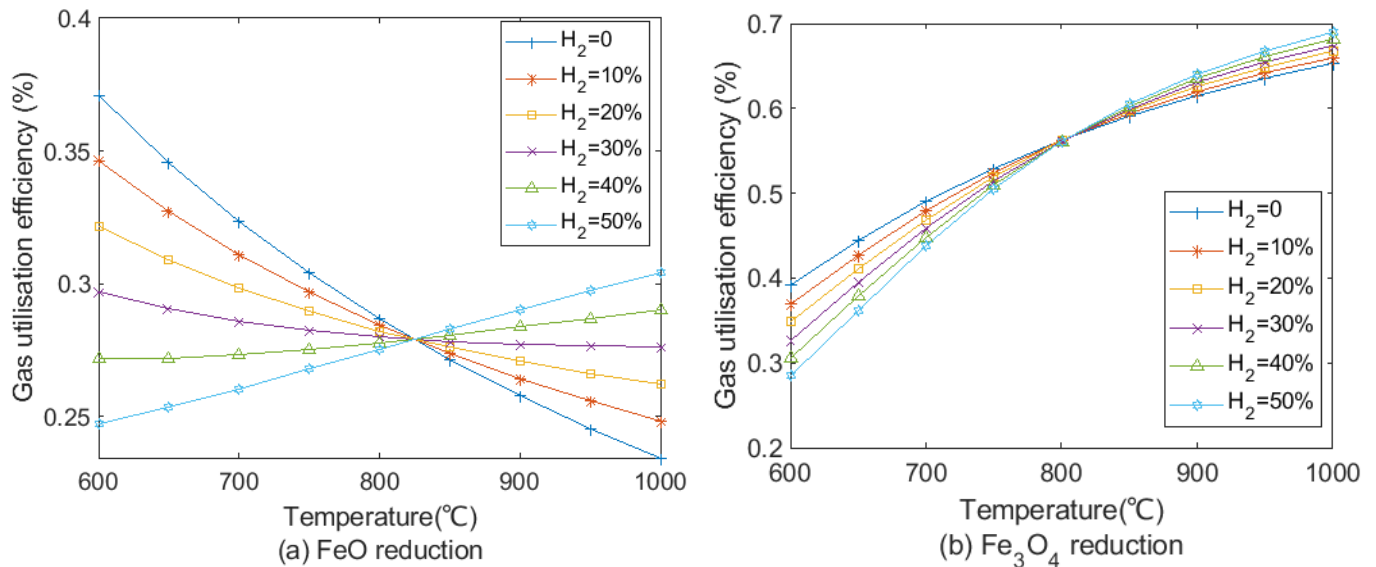


Figure 5. Gas utilisation efficiency at different H_2/CO ratio with temperature in (a) FeO and (b) Fe_3O_4 reductions.

Figure 5a presents the gas utilisation efficiency of FeO reduction. Due to the endothermic reaction of the H_2 reduction, utilisation efficiency of H_2 -rich reducing gas at 1000 °C for the FeO reduction increased from 23% with no H_2 to around 30% with 50% H_2 by the equal interval. When H_2 content was less than 30% in reducing gas, gas utilisation efficiency in FeO reduction decreased with the increase in temperature. In contrast, gas utilisation efficiency rose with temperature when H_2 content is more than 40% in reducing gas. Hence, H_2 content in the reducing gas should not be too low to hinder improvement in the gas utilisation efficiency. As shown in Figure 5b, since Fe_3O_4 reductions by CO and H_2 are endothermic, gas utilisation efficiency increases with temperature. The effect of increases in H_2 content for Fe_3O_4 reduction is less than FeO reduction in terms of gas utilisation efficiency. At 1000 °C, gas utilisation efficiency increases by less than 4% when H_2 content increases from 0% to 50%. The shaft gas injection temperature should be higher than 820 °C to promote gas utilisation in FeO and Fe_3O_4 reduction, especially focusing on FeO reduction.

3.2. BF Simulation Conditions and Validation

Without gas injection, the model developed in this work can be used for a traditional BF. The measured data collected from a 2500 m³ BF were used to validate this proposed model. The comparison of the industrial data and the model predictions is summarised in Table 2. The coke rate and top gas components were compared because they are essential measurable parameters that indicate the overall performance of an iron-making BF. The chemical composition of raw material data is shown in Tables 3–5. In general, results in this simulation show a similar trend as in practice, and the model was capable of estimating the overall iron-making process. The slight difference in top gas composition is because industrial data contain a slight amount of O_2 and CH_4 in top gas, which does not exist in this model.

Table 2. Quantitative validation of the model.

Parameter	Prediction	Industrial	Top Gas	Prediction	Industrial
Coke rate, kg/tHM	386	386	CO, %	25.1	24.9
Blast, Nm ³ /tHM	1060	1089	CO ₂ , %	21.1	20.0
Slag rate, kg/tHM	364	373	H ₂ , %	1.2	0.8
Burden input, kg/tHM	1676	1676	N ₂ , %	50.0	53
RAFT, °C	2205	2195	R _d	0.46	-

Table 3. Chemical composition of raw material and dust, $w/w\%$.

Composition	Tfe	FeO	SiO ₂	CaO	MgO	TiO ₂	S	Al ₂ O ₃
Sinter 1	55.85	9.59	5.25	10.35	2.19	0.17	0.03	2.5
Sinter 2	55.85	9.2	5.26	10.27	2.2	0.27	-	2.5
Pellet	61.92	1.46	5.31	1.45	-	1.58	-	0.98
Ti ore	40.27	-	9.07	2.05	-	10.78	-	1.69
Dust	39.80	2.58	4.05	2.04	0.83	0	-	1.31

Table 4. Chemical composition of coke and pulverised coal, $w/w\%$.

Composition	Fixed C	H ₂ O	FeO	CaO	SiO ₂	Al ₂ O ₃	MgO	N	O	H	S
Coke	86.06	4.50	1.6	0.39	4.49	3.69	0.35	0.30	0.21	0.33	1.80
PCI	71.15	0	0.03	1.98	8.4	7.93	0.18	0.34	3.16	2.10	0.30

Table 5. Chemical composition of hot metal, $w/w\%$.

Composition	Fe	C	Si	Mn	P	S	Ti
Hot metal	95.14	4.12	0.34	0.32	0.136	0.023	0.129

3.3. Effect of H₂ Injection on Coke Consumption Rate

The effect of injecting H₂-rich gas to hearth and/or shaft on coke rate is shown in Figure 6. The highest H₂ injection rate is limited to 160 m³/tHM to ensure a balanced energy distribution in the BF shaft. Injecting H₂ to the BF hearth shows less coke consumption than injecting it to the shaft. This is because it provides more sensible heat to the lower part of the furnace to compensate the heat supplied by coke combustion. The relationship between H₂ injection and coke consumption rate at 9% oxygen enrichment rate is given as in Equation (55). Injecting 7.9~10.9 m³/tHM H₂ can reduce the coke consumption rate by 1 kg/tHM, depending on the injection position.

$$K = 351X_{\text{shaft}} + 341X_{\text{hearth}} - (0.0913X_{\text{shaft}} + 0.1275X_{\text{hearth}}) \times H_{2\text{inj}} \quad (55)$$

where X_{shaft} and X_{hearth} are the proportion of H₂-rich gas injected to the shaft and hearth, respectively; and H_2 is the total H₂ injection volume to the BF, m³/tHM.

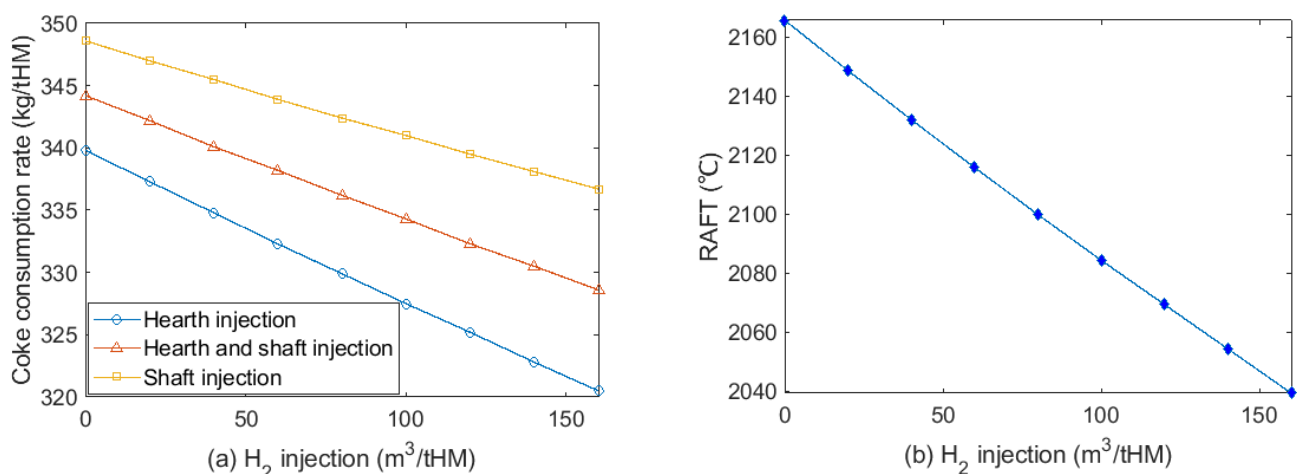


Figure 6. (a) Coke consumption rate at different H₂ injection volumes at different injection positions; (b) effect of H₂ injection to hearth on RAFT at 9% oxygen enrichment rate.

The effect of H₂ injection on RAFT at a constant oxygen enrichment rate is shown in Figure 6b. Injecting 20 m³/tHM H₂ can reduce RAFT by around 16 °C. Increasing oxygen

enrichment can achieve thermal compensation to maintain a stable RAFT and reduce coke consumption, as shown in Figure 7. Compared to the cases without thermal compensation, further reduction in coke consumption is obtained at 309 kg/tHM with 12.4% oxygen enrichment at 160 m³/tHM H₂ injection.

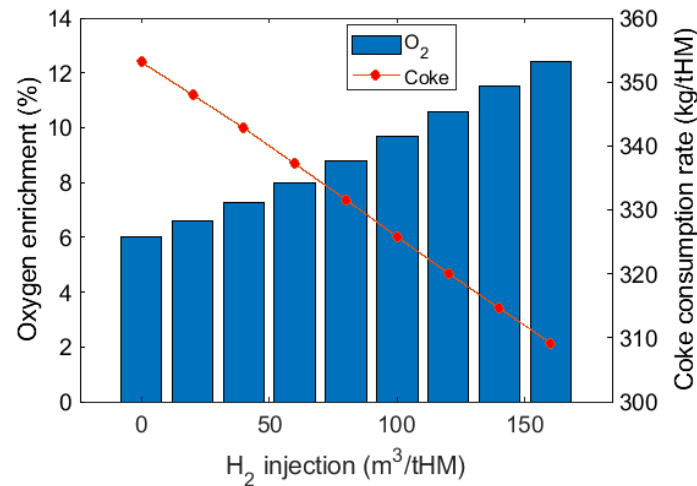


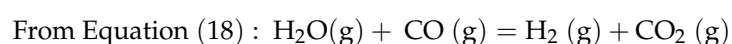
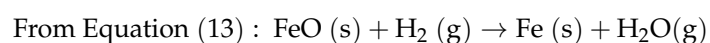
Figure 7. Coke consumption rate at different H₂ injection volumes at different oxygen enrichment rates for thermal compensation. RAFT was maintained at 2096 °C in this test.

3.4. Effect on H₂ Utilisation Efficiency

In the case of injecting H₂ to hearth, bosh gas composition is shown in Figure 8a. As the H₂ injection rate increased from 0 to 160 m³/tHM at a constant CO injection rate, CO content in bosh gas drops due to less coke consumption. N₂ content also decreased since less hot blast is required for carbon combustion. There was no H₂O in the bosh gas because H₂O that formed from the iron oxide reduction by H₂ reacted with coke to generate H₂ again at high temperature. The amount of top gas and its composition is described in Figure 8b. With more H₂ injection, the moisture content in the top gas increases slightly from 2.72% to 3.12% when the H₂ injection rate reaches from 0 to 100 m³/tHM. This is because H₂ utilisation efficiency significantly dropped from 72.6% to 22.9%, as shown in Figure 9a. CO content in top gas decreased because of less CO in the bosh gas and increased CO utilisation efficiency. CO₂ concentration was reduced by less than 2% because there was a significant drop of CO in the bosh gas and increase in CO utilisation efficiency is very limited. The H₂ injection promotes CO utilisation with the presence of the water–gas shift reaction. However, the overall effect of the water–gas shift reaction was very limited across the whole BF. The comprehensive gas utilisation efficiency gradually decreased from 43.6% to 39.0% when H₂ injection reached 160 m³/tHM.

H₂ and CO utilisation efficiency after thermal compensation is shown in Figure 9b. Results in this simulation reflect a similar trend as in the literature results [8,49]. Oxygen enrichment increased, and the nitrogen composition in the blast decreased with H₂ injection. Hence, there was more increase in reducing gas concentration than that in Figure 9a. With less N₂ dilution and stronger indirect reduction, CO utilisation with thermal compensation was enhanced by 5% with H₂ injection from 0 to 160 m³/tHM.

By H₂ increasing in the BF, CO utilisation increased, and H₂ utilisation efficiency decreased. One reason is that water–gas shift reaction Equation (18) would tend to proceed to the right-hand side, and both H₂ and CO₂ are generated in the upper furnace below 1000 °C. With the regeneration of H₂, FeO reduction in Equation (7) can be considered to be proceeding in two successive stages, as shown in Equations (13) and (18):



From Equation (7) : Overall : $\text{FeO (s)} + \text{CO (g)} \rightarrow \text{Fe (s)} + \text{CO}_2 \text{ (g)}$

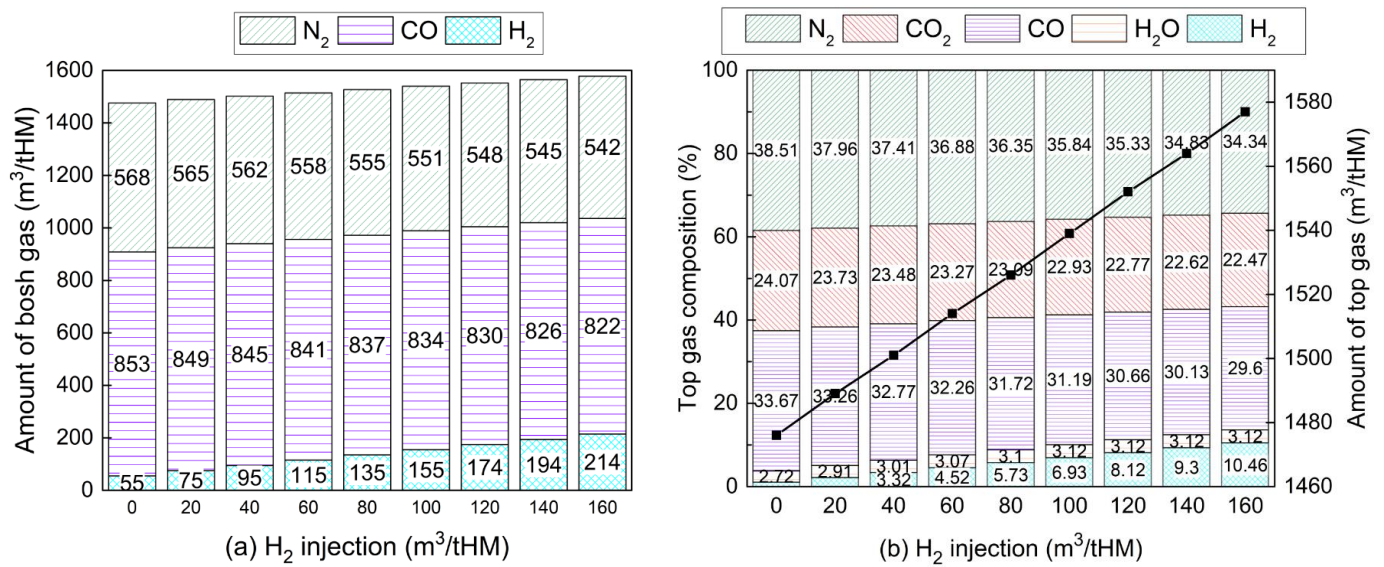


Figure 8. Variations of (a) bosh gas and (b) top gas composition with hydrogen injection. (H₂ injection at 0 m³/tHM indicates the operating condition of a traditional BF with oxygen enrichment rate at 9%).

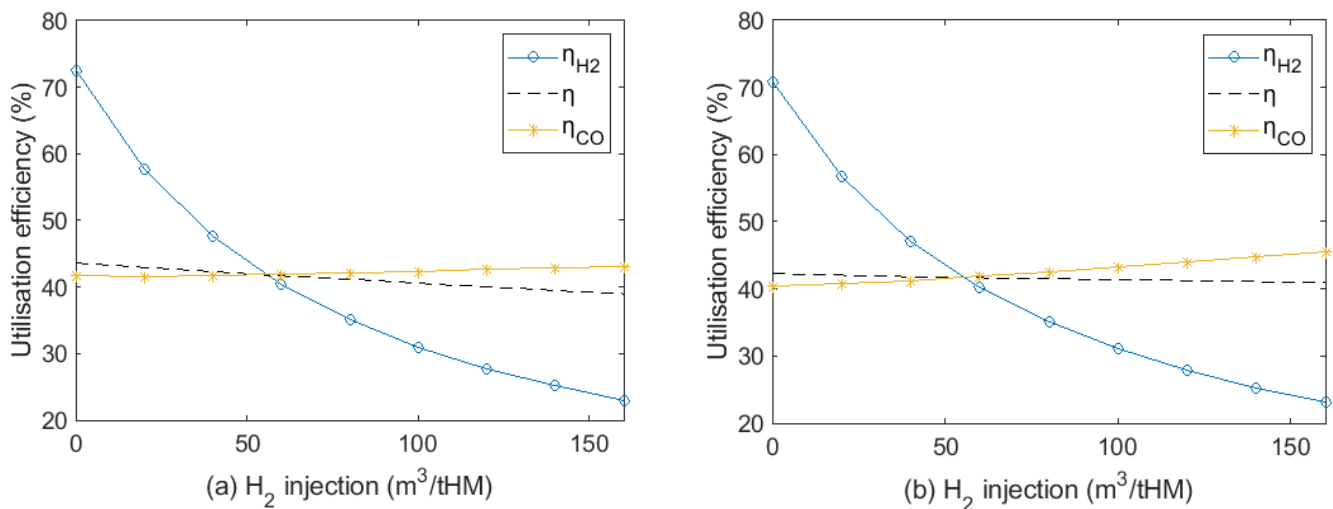


Figure 9. Variations in gas utilisation efficiency with hydrogen injection (a) before and (b) after thermal compensation.

Due to the smaller size and high diffusivity of H₂, the reaction in Equation (13) has an advantage over the reaction in Equation (7). Thus, FeO reduction by CO was promoted by increased H₂ content.

As depicted in Figure 10, with H₂ injection and thermal compensation, the degree of indirect reduction increased because H₂ reduction replaced part of the direct reduction and oxygen enrichment enhanced reducing gas atmosphere. Since the direct reduction was a huge endothermic reaction process in the lower furnace, less direct reduction reduces coke consumption. Compared to the higher H₂ injection volume, injecting 0 to 80 m³/tHM H₂ generates more effect on the degree of indirect reduction, from 0.107 to 0.125. Further, the injection of more than 50 m³/tHM H₂ significantly increased the indirect reduction of CO. Considering gas utilisation efficiency, H₂ injection should be around 50–80 m³/tHM to maintain smooth BF operation and avoid too much excess H₂ in top gas.

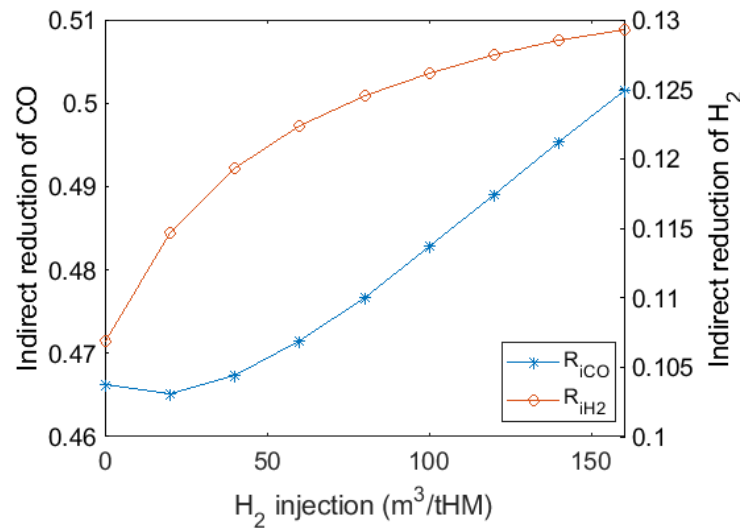


Figure 10. Variations in degree of indirect reduction by CO and H₂ with H₂ injection and thermal compensation.

3.5. Effects on CO₂ Emissions and Energy Consumption

In this work, the CO injected into the BF comes from the CO₂ captured in top gas, which reduces CO₂ emission compared to a traditional BF process. The emission from CCU can be negligible because it applies renewable electricity. The total emission of this iron-making process includes uncaptured CO₂, flue gases from BFG combusted in the preheater and the hot blast stoves, which is shown in Figure 11a. The main CO₂ emission reduction comes from the hot stoves. Compared with the traditional BF iron-making system that lacks CCU and gas injection, CO₂ emission dropped from 534 to around 272 m³/tHM with 160 m³/tHM H₂ injection in this system. When increasing H₂ content from 0 to 80 m³/tHM, CO₂ emission only decreased by 20 m³/tHM because more BFG was consumed to preheat the injection gas. Additionally, injecting H₂-rich gas into the shaft showed more CO₂ emission reduction capability than injecting H₂ into a hearth or both tuyeres, as shown in Figure 11b.

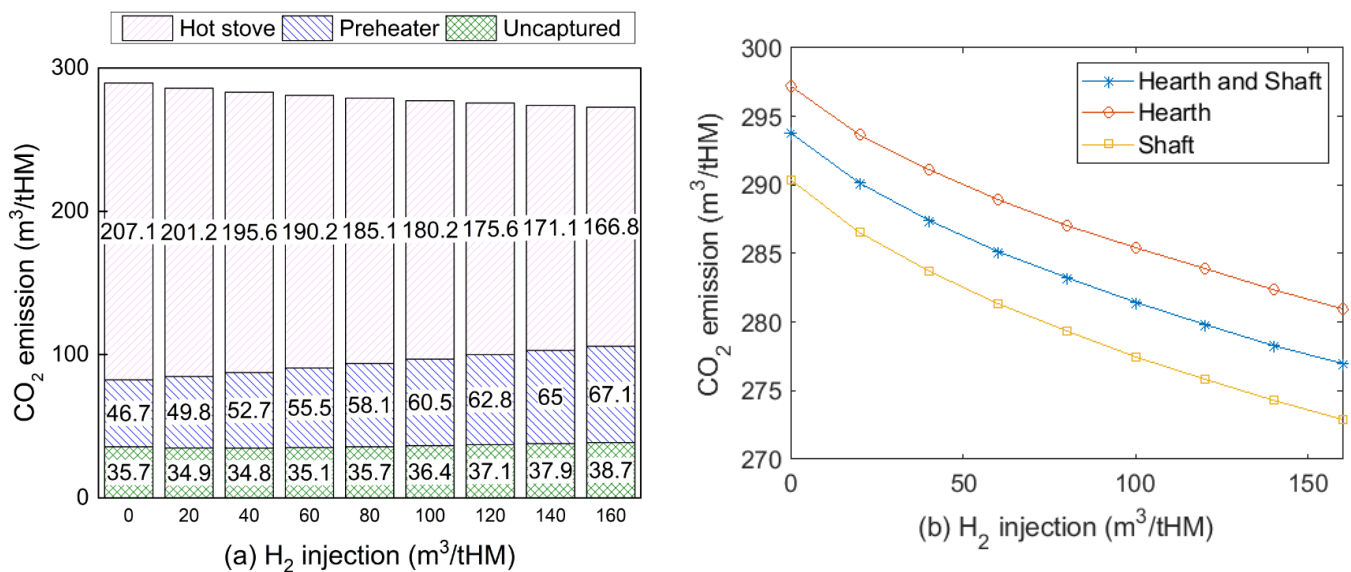


Figure 11. CO₂ emissions of iron-making process with H₂ injection (a) with different CO₂ emission sources for shaft injection case; (b) at different injection positions (injection temperature for shaft and hearth was 900 and 1250 °C, respectively).

The energy consumption of the process described in Figure 1 was calculated on the basis of static mass and energy balance, using Equation (56). The standard coal coefficient for each substance in a kilogram of coal equivalent per ton of hot metal (kgce/tHM) is used in this analysis [50].

$$E_{net} = E_{coke} + E_{PC} + E_{BOFG} + E_{blast} + E_{cap} + E_{conv} + E_{water} - E_{export} - E_{O_2} \quad (56)$$

where E_{net} is the net energy consumption of the process; E_{coke} is the energy input by coke; E_{PC} is the energy input by pulverised coal; E_{BOFG} is the energy input by BOFG to the hot blast stoves; E_{blast} is the energy carried by the blast to hot blast stoves; E_{cap} is the electricity required for CO₂ capture unit; E_{conv} is the electricity required for CO₂ electrolyser, as calculated by Equation (2); E_{water} is the energy carried by the make-up water required at the humidifier for H₂ generation in the electrolyser; E_{export} is the energy carried by the BFG that is exported to other processes in the integrated steel mill; and E_{O_2} is the energy carried by the oxygen that is generated in the electrolyser and exported to other processes in the integrated steel mill.

Energy consumption results are shown in Figure 12. In a traditional BF, carbon resources from coke and pulverised coal injection provide the primary energy input, which accounts for 80% in total. When hydrogen is injected into the BF from 0 to 160 m³/tHM, carbon only accounts for 65% to 50% of the total energy consumption. With H₂-rich gas injection from 0 to 160 m³/tHM, net energy consumption increased from 541 to 698 kgce/tHM, which is higher than that of the traditional BF (504 kgce/tHM) because electricity required for CO₂ conversion to generate H₂ kept increasing from 158 to 369 kgce/tHM.

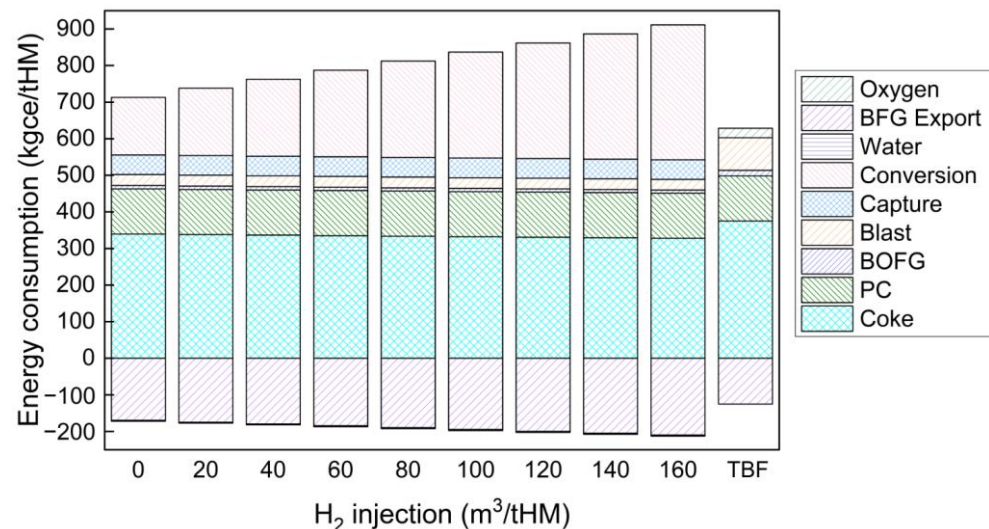


Figure 12. Energy consumption for H₂-rich gas injection BF and traditional BF process (energy carried by the make-up water needed for the CO₂ conversion and by BOFG was less than 1% of total energy consumption and thus not indicated in this figure).

In summary, increasing hydrogen injection volume can reduce coke consumption and CO₂ emissions. For coke consumption and CO₂ emission reduction, the hydrogen injection amount should be as much as possible, as long as it satisfies the energy balance in the BF. In this case, the hydrogen injection amount should be 160 m³/tHM. However, injecting too much H₂ significantly reduces its utilisation efficiency and increases the net energy consumption of this process. Further study is recommended to develop a multiobjective optimisation model to balance these effects of hydrogen injection. In general, injecting H₂ at around 80 m³/tHM may consume less energy and suppress CO₂ emissions under the simulation conditions.

Energy consumption to produce 1 tonne of hot metal in the case of injecting 80 m³/tHM H₂ with 200 m³/tHM CO is indicated in Figure 13. Compared to the traditional BF as

indicated by Table 2, coke consumption decreased by 43 kg/tHM. CO₂ emission dropped from 534 m³/tHM for a traditional BF to 278 m³/tHM in this case (including gas heating flue gas, capture unit CO₂ letdown, and stack flue gas). However, electricity consumption in the CO₂ capture unit and electrolyser is one of the largest energy inputs. The economic impact of this CCU technology as an auxiliary system to the BF is highly recommended for future investigation.

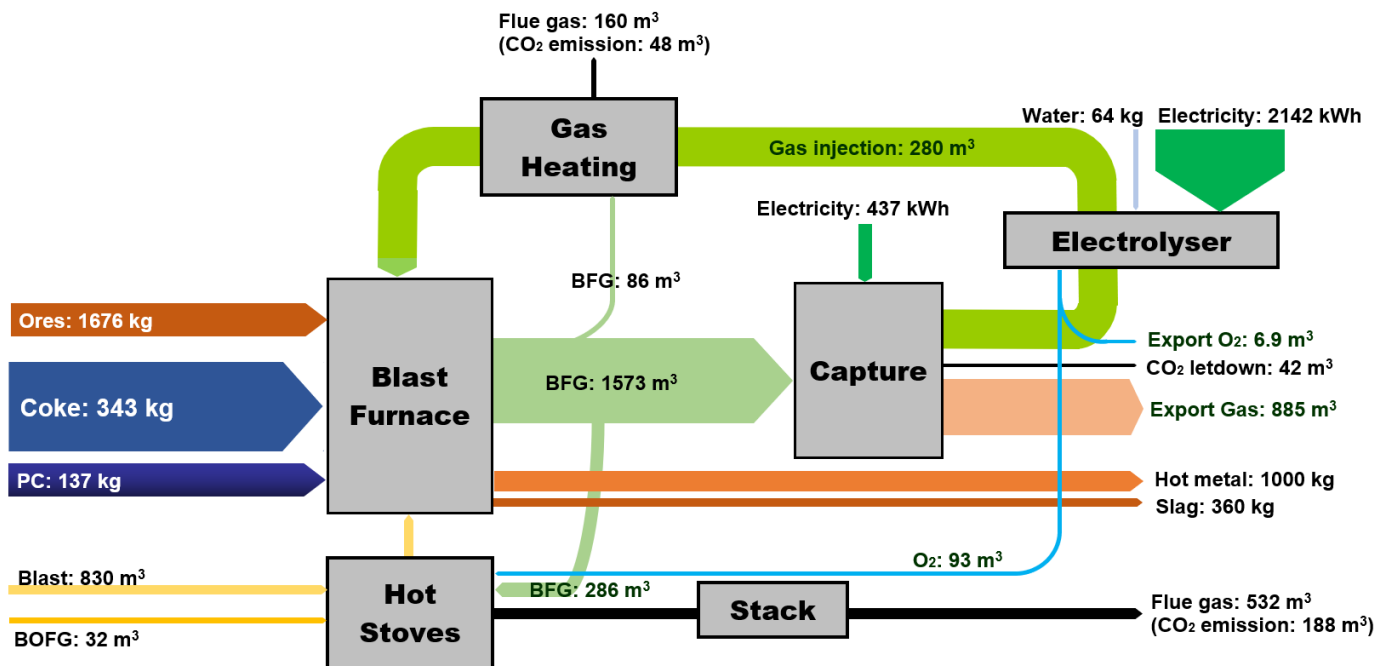


Figure 13. Energy and material consumption of the process with 80 m³/tHM hydrogen injection. Relative flow size estimated by energy and demonstrated as bar width.

4. Conclusions

In this study, a thermodynamic model was used to determine the utilisation efficiency of H₂-rich gas by considering H₂ behaviour at different reduction stages. A static mass and energy balance model of the BF was adopted with this thermodynamic model. The effect of injecting H₂-rich gas on BF performance was determined in terms of its coke consumption, CO₂ emissions, and energy consumption. Under these simulation conditions, the major findings of this study were:

1. The desired shaft gas injection temperature should not exceed 1000 °C to suppress the endothermic FeO reduction reaction by H₂-rich gas.
2. Injecting H₂ to BF hearth has a better effect on coke rate reduction than that of injection to the shaft. The lowest H₂ consumption to save 1 kg of coke was estimated to be 7.9 m³/tHM.
3. H₂ utilisation efficiency dropped significantly with increasing H₂ content, and the increase in CO utilisation efficiency was limited. Further research should focus on improving H₂ utilisation efficiency with a high H₂ injection rate.
4. Considering H₂ utilisation efficiency and the degree of indirect reduction by H₂ and CO, the proper H₂ injection rate should be from around 50 to 80 m³/tHM.
5. Introducing H₂-rich gas injection can reduce CO₂ emissions of the iron-making process by up to 262 m³/tHM compared with a traditional BF. However, injecting too much H₂ would hinder CO₂ emission reduction due to its requirement of preheating outside the BF.
6. The energy consumption of this proposed process was higher than that of the traditional BF. Although coke consumption was reduced by 43 kg/tHM more than that of the traditional BF, net energy consumption increased with the amount of injected

hydrogen due to the high electricity consumption in the CO₂ capture and electrolyser. Developing a CO₂ conversion unit with higher efficiency but less energy consumption is strongly recommended.

Author Contributions: Conceptualization, Y.H., T.E.R., V.R. and G.W.; methodology, Y.H. and G.W.; software, Y.H.; validation, Y.H. and L.H.; formal analysis, Y.H.; investigation, Y.H., Y.Q., J.C. and L.H. resources, L.H.; data curation, Y.H.; writing—original draft preparation, Y.H.; writing—review and editing, Y.H., Y.Q., J.C., L.H., T.E.R. and G.W.; visualization, Y.H.; supervision, T.E.R., V.R. and G.W.; project administration, G.W. and L.H.; funding acquisition, L.H. All authors have read and agreed to the published version of the manuscript.

Funding: This research was funded by HBIS (China) grant number ICSS2017-04.

Institutional Review Board Statement: Not applicable.

Informed Consent Statement: Not applicable.

Data Availability Statement: Data sharing not applicable. No new data were created or analysed in this study. Data sharing is not applicable to this article.

Acknowledgments: The authors gratefully acknowledge HBIS Group Company Limited for funding support and the scholarship support from the University of Queensland.

Conflicts of Interest: The authors declare no conflict of interest.

Nomenclature

Abbreviations

BF	Blast furnace
PCI	Pulverised coal injection
CCU	CO ₂ capture and conversion unit
RAFT	Raceway adiabatic flame temperature
tHM	Tonne of hot metal

Roman and Greek symbols

E	Energy, kWh/tHM or kgce/tHM
V	Volume of gas, m ³ /tHM
T	Temperature, °C
C _i	Specific heat capacity, kJ/m ³ ·°C
K _i	Reaction equilibrium constant of reduction stage i; i = I, II, III
G	Gibbs free energy, kJ/mol
φ	Volume fraction of gas component
η _{iCO}	Utilisation efficiency of CO in stage i, i = 1, 2, 3
η _{iH₂}	Utilisation efficiency of H ₂ in stage i, i = 1, 2, 3
n	Minimal CO required for iron ores reduction, mol
m	Minimal H ₂ required for iron ores reduction, mol
X _i	Volume reaction of CO or H ₂ in reducing gas entering the BF shaft
η	Overall gas utilisation efficiency for H ₂ -rich reducing gas in the BF
%(Reducing gas)	Proportion of H ₂ and CO in the total amount of gas entering the bosh and shaft.
Q	Sensible heat of material, kJ/tHM
H	Enthalpy of material, kJ/tHM
R _d	Degree of direct reduction
r _i	Degree of indirect reduction
(Fe) _{HM}	Iron content in hot metal
ΔH ⁰	Enthalpy of reaction, kJ/tHM
w	Weight fraction of solid material
H _{2inj}	Total H ₂ injection volume to the BF, m ³ /tHM

References

1. Xu, K. Low carbon economy and iron and steel industry. *Iron Steel* **2010**, *45*, 1–12.
2. Pardo, N.; Moya, J.A. Prospective scenarios on energy efficiency and CO₂ emissions in the European Iron & Steel industry. *Energy* **2013**, *54*, 113–128. [[CrossRef](#)]
3. Babich, A.; Senk, D. *New Trends in Coal Conversion: Combustion, Gasification, Emissions, and Coking*; Woodhead Publishing: Sawson, UK, 2019; pp. 367–404.
4. Danloy, G.; Berthelemot, A.; Grant, M.; Borlée, J.; Sert, D.; Van Der Stel, J.; Jak, H.; Dimastromatteo, V.; Hallin, M.; Eklund, N.; et al. ULCOS-Pilot testing of the Low-CO₂ Blast Furnace process at the experimental BF in Luleå. *Rev. Metall.-Int. J. Metall.* **2009**, *106*, 1–8. [[CrossRef](#)]
5. Knop, K.; Hallin, M.; Burstrom, E. ULCORED SP 12 Concept for minimized CO₂ emission. *Metall. Res. Technol.* **2009**, *106*, 419–421. [[CrossRef](#)]
6. Material Economics. Industrial Transformation 2050: Pathways to Net-Zero Emisions from EU Heavy Industry. 2019. Available online: <https://materialeconomics.com/publications/industrial-transformation-2050> (accessed on 8 January 2022).
7. Chisalita, D.-A.; Petrescu, L.; Cobden, P.; van Dijk, H.E.; Cormos, A.-M.; Cormos, C.-C. Assessing the environmental impact of an integrated steel mill with post-combustion CO₂ capture and storage using the LCA methodology. *J. Clean. Prod.* **2019**, *211*, 1015–1025. [[CrossRef](#)]
8. Nogami, H.; Kashiwaya, Y.; Yamada, D. Simulation of Blast Furnace Operation with Intensive Hydrogen Injection. *ISIJ Int.* **2012**, *52*, 1523–1527. [[CrossRef](#)]
9. Usui, T.; Kawabata, H.; Ono-Nakazato, H.; Kurosaka, A. Fundamental Experiments on the H₂ Gas Injection into the Lower Part of a Blast Furnace Shaft. *ISIJ Int.* **2002**, *42*, S14–S18. [[CrossRef](#)]
10. Pinegar, H.K.; Moats, M.S.; Sohn, H.Y. Process Simulation and Economic Feasibility Analysis for a Hydrogen-Based Novel Suspension Ironmaking Technology. *Steel Res. Int.* **2011**, *82*, 951–963. [[CrossRef](#)]
11. Wagner, D.; Devisme, O.; Patisson, F.; Ablitzer, D. A laboratory study of the reduction of iron oxides by hydrogen. *arXiv* **2008**, arXiv:08032831.
12. Spreitzer, D.; Schenk, J. Reduction of Iron Oxides with Hydrogen—A Review. *Steel Res. Int.* **2019**, *90*, 1900108. [[CrossRef](#)]
13. Qie, Y.; Lyu, Q.; Li, J.; Lan, C.; Liu, X. Effect of Hydrogen Addition on Reduction Kinetics of Iron Oxides in Gas-injection BF. *ISIJ Int.* **2017**, *57*, 404–412. [[CrossRef](#)]
14. Zuo, H.-b.; Wang, C.; Dong, J.-j.; Jiao, K.-x.; Xu, R.-s. Reduction kinetics of iron oxide pellets with H₂ and CO mixtures. *Int. J. Miner. Metall. Mater.* **2015**, *22*, 688–696. [[CrossRef](#)]
15. Chu, M.; Nogami, H.; Yagi, J.-I. Numerical Analysis on Injection of Hydrogen Bearing Materials into Blast Furnace. *ISIJ Int.* **2004**, *44*, 801–808. [[CrossRef](#)]
16. Yilmaz, C.; Wendelstorf, J.; Turek, T. Modeling and simulation of hydrogen injection into a blast furnace to reduce carbon dioxide emissions. *J. Clean. Prod.* **2017**, *154*, 488–501. [[CrossRef](#)]
17. Lyu, Q.; Qie, Y.; Liu, X.; Lan, C.; Li, J.; Liu, S. Effect of hydrogen addition on reduction behavior of iron oxides in gas-injection blast furnace. *Thermochim. Acta* **2017**, *648*, 79–90. [[CrossRef](#)]
18. Watakabe, S.; Miyagawa, K.; Matsuzaki, S.; Inada, T.; Tomita, Y.; Saito, K.; Osame, M.; Sikström, P.; Ökvist, L.S.; Wikstrom, J.-O. Operation Trial of Hydrogenous Gas Injection of COURSE50 Project at an Experimental Blast Furnace. *ISIJ Int.* **2013**, *53*, 2065–2071. [[CrossRef](#)]
19. Qie, Y.; Lyu, Q.; Liu, X.; Li, J.; Lan, C.; Zhang, S.; Yan, C. Effect of Hydrogen Addition on Softening and Melting Reduction Behaviors of Ferrous Burden in Gas-Injection Blast Furnace. *Met. Mater. Trans. A* **2018**, *49*, 2622–2632. [[CrossRef](#)]
20. Wang, Y.; He, Z.-J.; Zhang, W.-l.; Zhu, H.-b.; Zhang, J.-h.; Pang, Q.-h. Reduction behavior of iron-bearing burdens in hydrogen-rich stream. *Iron Steel* **2020**, *55*, 34–40.
21. Andersson, J.; Grönkvist, S. A comparison of two hydrogen storages in a fossil-free direct reduced iron process. *Int. J. Hydrog. Energy* **2021**, *46*, 28657–28674. [[CrossRef](#)]
22. Hydrogen Council. Path to Hydrogen Competitiveness: A Cost Perspective. 2020. Available online: <https://hydrogencouncil.com/en/path-to-hydrogen-competitiveness-a-cost-perspective/> (accessed on 8 January 2022).
23. Uribe-Soto, W.; Portha, J.-F.; Commenge, J.-M.; Falk, L. A review of thermochemical processes and technologies to use steelworks off-gases. *Renew. Sustain. Energy Rev.* **2017**, *74*, 809–823. [[CrossRef](#)]
24. Da Rocha, E.P.; Guilherme, V.S.; de Castro, J.A.; Sasaki, Y.; Yagi, J.-I. Analysis of synthetic natural gas injection into charcoal blast furnace. *J. Mater. Res. Technol.* **2013**, *2*, 255–262. [[CrossRef](#)]
25. Halim, K.S.A. Theoretical Approach to Change Blast Furnace Regime with Natural Gas Injection. *J. Iron Steel Res. Int.* **2013**, *20*, 40–46. [[CrossRef](#)]
26. Trinkel, V.; Kieberger, N.; Bürgler, T.; Rechberger, H.; Fellner, J. Influence of waste plastic utilisation in blast furnace on heavy metal emissions. *J. Clean. Prod.* **2015**, *94*, 312–320. [[CrossRef](#)]
27. Domingo-Tafalla, B.; Martínez-Ferrero, E.; Franco, F.; Palomares-Gil, E. Applications of Carbon Dots for the Photocatalytic and Electrocatalytic Reduction of CO₂. *Molecules* **2022**, *27*, 1081. [[CrossRef](#)]
28. Zhong, H.; Sa, R.; Lv, H.; Yang, S.; Yuan, D.; Wang, X.; Wang, R. Covalent organic framework hosting metalloporphyrin-based carbon dots for visible-light-driven selective CO₂ reduction. *Adv. Funct. Mater.* **2020**, *30*, 2002654. [[CrossRef](#)]

29. Kungas, R. Review—Electrochemical CO₂ Reduction for CO Production: Comparison of Low- and High-Temperature Electrolysis Technologies. *J. Electrochem. Soc.* **2020**, *167*, 044508. [CrossRef]
30. Parvanian, A.M.; Sadeghi, N.; Rafiee, A.; Shearer, C.J.; Jafarian, M. Application of porous materials for CO₂ reutilization: A Review. *Energies* **2022**, *15*, 63. [CrossRef]
31. Delacourt, C.; Ridgway, P.; Kerr, J.; Newman, J. Design of an Electrochemical Cell Making Syngas (CO + H₂) from CO₂ and H₂O reduction at Room Temperature. *J. Electrochem. Soc.* **2007**, *155*, B42. [CrossRef]
32. Lu, Q.; Jiao, F. Electrochemical CO₂ reduction: Electrocatalyst, reaction mechanism, and process engineering. *Nano Energy* **2016**, *29*, 439–456. [CrossRef]
33. Garg, S.; Li, M.; Idros, M.N.; Wu, Y.; Wang, G.; Rufford, T.E. Is Maximising Current Density Always the Optimum Strategy in Electrolyser Design for Electrochemical CO₂ Conversion to Chemicals? 2021. Available online: <https://chemrxiv.org/engage/chemrxiv/article-details/61a7235f7848050092a110b4> (accessed on 8 January 2022).
34. De Ras, K.; Van de Vijver, R.; Galvita, V.V.; Marin, G.B.; Van Geem, K.M. Carbon capture and utilization in the steel industry: Challenges and opportunities for chemical engineering. *Curr. Opin. Chem. Eng.* **2019**, *26*, 81–87. [CrossRef]
35. De Castro, J.A.; Takano, C.; Yagi, J.-i. A theoretical study using the multiphase numerical simulation technique for effective use of H₂ as blast furnaces fuel. *J. Mater. Res. Technol.* **2017**, *6*, 258–270. [CrossRef]
36. Zhang, W. Fundamental Study and Process Optimization of the Oxygen Blast Furnace Ironmaking. Doctoral Dissertation, Northeastern University, Shenyang, China, 2015.
37. Kwak, N.-S.; Lee, J.H.; Lee, I.Y.; Jang, K.R.; Shim, J.-G. A study of the CO₂ capture pilot plant by amine absorption. *Energy* **2012**, *47*, 41–46. [CrossRef]
38. Bui, M.; Adjiman, C.S.; Bardow, A.; Anthony, E.J.; Boston, A.; Brown, S.; Fennell, P.S.; Fuss, S.; Galindo, A.; Hackett, L.A.; et al. Carbon capture and storage (CCS): The way forward. *Energy Environ. Sci.* **2018**, *11*, 1062–1176. [CrossRef]
39. Choi, J.; Cho, H.; Yun, S.; Jang, M.-G.; Oh, S.-Y.; Binns, M.; Kim, J.-K. Process design and optimization of MEA-based CO₂ capture processes for non-power industries. *Energy* **2019**, *185*, 971–980. [CrossRef]
40. Hari, S.R.; Balaji, C.P.; Karunamurthy, K. Carbon Capture and Storage Using Renewable Energy Sources: A Review. *IOP Conf. Ser. Earth Environ. Sci.* **2020**, *573*, 12004. [CrossRef]
41. Aresta, M.; Dibenedetto, A.; Angelini, A. The use of solar energy can enhance the conversion of carbon dioxide into energy-rich products: Stepping towards artificial photosynthesis. *Philos. Trans. R. Soc. London. Ser. A Math. Phys. Eng. Sci.* **2013**, *371*, 20120111. [CrossRef]
42. McBrien, M.; Serrenho, A.C.; Allwood, J. Potential for energy savings by heat recovery in an integrated steel supply chain. *Appl. Therm. Eng.* **2016**, *103*, 592–606. [CrossRef]
43. Mazanek, E.; Jasienska, S.; Brachucy, A.; Bryk, C. The influence of hydrogen in the gas mixture of hydrogen and CO on the dynamics of the reduction process. *Metal. Odlew.* **1982**, *8*, 53–70.
44. Piotrowski, K.; Mondal, K.; Lorethova, H.; Stonawski, L.; Szymanski, T.; Wiltowski, T. Effect of gas composition on the kinetics of iron oxide reduction in a hydrogen production process. *Int. J. Hydrog. Energy* **2005**, *30*, 1543–1554. [CrossRef]
45. Jozwiak, W.; Kaczmarek, E.; Maniecki, T.; Ignaczak, W.; Maniukiewicz, W. Reduction behavior of iron oxides in hydrogen and carbon monoxide atmospheres. *Appl. Catal. A Gen.* **2007**, *326*, 17–27. [CrossRef]
46. Wu, S.; Wang, X.; Zhang, J. *Ferrous Metallurgy*; Metallurgical Industry Press: Beijing, China, 2019; pp. 46–48.
47. Bernasowski, M. Theoretical Study of the Hydrogen Influence on Iron Oxides Reduction at the Blast Furnace Process. *Steel Res. Int.* **2014**, *85*, 670–678. [CrossRef]
48. Li, J.; Wang, P.; Zhou, L.; Cheng, M. The Reduction of Wustite with High Oxygen Enrichment and High Injection of Hydrogenous Fuel. *ISIJ Int.* **2007**, *47*, 1097–1101. [CrossRef]
49. Tang, J.; Chu, M.; Li, F.; Zhang, Z.; Tang, Y.; Liu, Z.; Yagi, J. Mathematical simulation and life cycle assessment of blast furnace operation with hydrogen injection under constant pulverized coal injection. *J. Clean. Prod.* **2021**, *278*, 123191. [CrossRef]
50. *China GB/T 2589-2020*; General Principles for Calculation of the Comprehensive Energy Consumption. Standardization Administration of China: Beijing, China, 2020.